Mechanism and Machine Theory 44 (2009) 1485–1496

Contents lists available at ScienceDirect

Mechanism and Machine Theory

journal homepage: www.elsevier.com/locate/mechmt

Kinematic modeling of a 5-DOF parallel mechanism for semi-spherical workspace

O. Piccin [a,*], B. Bayle [a], B. Maurin [b], M. de Mathelin [a]

[a] LSIIT, UMR CNRS 7005, University of Strasbourg, France
[b] Cerebellum Automation, Chavanod, France

ARTICLE INFO

Article history:
Received 29 January 2008
Received in revised form 12 November 2008
Accepted 26 November 2008
Available online 13 January 2009

Keywords:
Lower-mobility parallel mechanism
Spherical workspace manipulator

ABSTRACT

This paper presents the architecture synthesis and the kinematic modeling of a new five-degree-of-freedom parallel manipulator. The proposed mechanism is a 3T2R device intended to position and orient a line in space. It has been originally designed for a medical application in which the aforementioned line corresponds to the axis of a surgical needle. The mechanism is characterized by an asymmetric arrangement of its legs and wider mobility ranges than usually obtained with a parallel structure. Its inverse and forward kinematic models are derived, together with the assembly modes complying with the practical limitations of the mechanism.

1. Introduction

Medical interventions and particularly minimally invasive surgery have become an important application field of robotics. While pioneer achievements mainly involved off-the-shelf robotic manipulators or modified industrial arms, it is now well established that the functions required for a given medical application are better performed with a specialized mechanical structure. The mechanism presented in this paper is part of a robotic assistant developed for the diagnosis and therapy of tumors in the context of interventional radiology [1,2]. This system is designed so as to perform teleoperated percutaneous needle insertions under medical image guidance. It is based on an original robotic platform, which positions and orients a needle insertion tool.

There have already been a few systems developed for interventional radiology, generally based on a platform on which a needle insertion device is mounted. The PAKY system [3] and the AcuBot [4] are among the first systems compatible with computed tomography (CT). The PAKY is based on a remote center of motion (RCM) device serially mounted on a passive arm attached to the operation bed. The AcuBot system adds to the PAKY a pre-positioning stage for the coarse placement near the intervention site. The innomotion robot [5] also features a RCM structure. A passive holder with two degrees of freedom (DOF) is used to position the actuated system in an optimal way given the shape and the volume of CT-scanners and MRI machines to which it is compatible. The B-Rob I [6] is a CT-compatible robotic system for robot-assisted biopsy based on a PPPR structure to obtain the coarse positioning of the needle near the entry point and a 3-DOF needle positioning unit to achieve the fine orientation of the needle. For these two previous systems, the needle is inserted manually. The LPR [7] is a 5-DOF patient-mounted robot compatible with MRI. Two DOF are obtained with motorized linear translations at the surface of the patient body. The orientation at the entry point and the insertion are obtained with pneumatic actuators driving two intersecting revolute joints and a prismatic pair along the needle axis. The MrBot [8] is a 3T3R parallel structure holding a 1-DOF needle driver for prostate percutaneous procedures. This robot is a 5-legged platform with a 4UPS-UPU architecture.

* Corresponding author.
E-mail address: Olivier.Piccin@insa-strasbourg.fr (O. Piccin).

0094-114X/$ - see front matter © 2008 Elsevier Ltd. All rights reserved.
doi:10.1016/j.mechmachtheory.2008.11.012

Like the previous systems, the developed robotic device must allow to position and orient the axis of a surgical needle as planned by the clinician. The mobilities required to insert the needle in the pointed anatomical target are provided by a separate tool not described in this document.

It is important to identify the associated medical constraints to perform the mechanism synthesis [9]. Percutaneous needle insertions require image guidance to complete safely. At the moment, the most widely used imaging modality is computed tomography. During an intervention the patient is placed within the ring of the CT scanner. To cope with security constraints and provide a natural compensation of accidental motions of the patient, e.g. coughing, the proposed mechanism is mounted on the patient's body to which it is strapped [2]. The free space within the CT-scanner tunnel can be assimilated to a semi-spherical zone with a radius of 200 mm, centered at the entry point. The mobility imposed by the access to the organs requires a large needle incidence: 0–65° in the CT-scanner plane and ±25° in the perpendicular plane. Another important feature is the possibility to change the entry point position on the patient's skin within a range of ±10 mm around a predefined point. To our knowledge, none of the existing robots dedicated to needle placement fulfills all these demanding mobility requirements.

This paper presents the architecture synthesis and the kinematic modeling of a system designed to comply with the previous constraints. It is a novel 5-DOF parallel mechanism, with an asymmetric structure. Though relatively complex the closed-form of both the inverse and forward kinematic models can be derived. The text is organized as follows. In Section 2, the mechanism design is derived from a kinematic decomposition of the task performed by the robot. Then, the designed structure is parameterized in Section 3 and the inverse and forward kinematic models are calculated in Section 4. Finally, Section 5 discusses the conclusions and the perspectives of this work.

2. Architecture synthesis

2.1. Required mobilities and synthesis

We considered candidate systems with five DOF in order to position and orient a line in space. Serial mechanisms were found to be inappropriate for our application, mainly because of their inherent flexibility. In contrast, parallel mechanisms like Gough-Stewart platforms exhibit a higher stiffness and a better working accuracy, but are limited by a small workspace, a higher design complexity and a difficult forward kinematic modeling. To overcome some of these shortcomings, research on lower-mobility parallel mechanisms has recently drawn a lot of interest [10–12] but most of the proposed mechanisms have fully-symmetrical architectures [13,14]. For such mechanisms, type synthesis based on the constraint-synthesis method [15] or the Lie subgroup synthesis method [16,17] are quite powerful to enumerate every parallel candidate mechanisms with identical legs structures. However, to cope with specific requirements like the ones of our application, it is interesting to consider also asymmetric mechanisms with different sorts of legs. Then, the number of possible structures increases rapidly and a specific method has to be used.

In order to obtain the most promising lower-mobility parallel mechanisms with 3T2R mobility, we introduce a kinematic decomposition of the task. Let $\mathscr{F}_0 = (O_0, \boldsymbol{x}_0, \boldsymbol{y}_0, \boldsymbol{z}_0)$ and $\mathscr{F}_f = (O_f, \boldsymbol{x}_f, \boldsymbol{y}_f, \boldsymbol{z}_f)$ be respectively the base and the platform frames of the mechanism to be synthesized. The line $\mathscr{L}$ to be positioned and oriented is defined by the axis $(O_f, \boldsymbol{z}_f)$. Let (M) be a moving plane passing through the axis $(O_0, \boldsymbol{y}_0)$ and containing O_f. As the mechanism has five DOF and does not need to set the rotation of the line $\mathscr{L}$ about its axis, the axis $(O_f, \boldsymbol{y}_f)$ can be defined without loss of generality in order to lie in (M).

Under these assumptions, the transformation from frame $\mathscr{F}_0$ to frame $\mathscr{F}_f$ can be decomposed as follows (Fig. 1):

$$\mathscr{F}_0 \overset{\mathrm{Rot}(\boldsymbol{y}_0,\varphi)}{\rightarrow} \mathscr{F}_\varphi \underbrace{\overset{\mathrm{Tr}(\boldsymbol{y}_\varphi,t_1)\mathrm{Tr}(\boldsymbol{z}_\varphi,t_2)\mathrm{Rot}(\boldsymbol{x}_\varphi,\psi)}{\longrightarrow}}_{\text{position and orientation in } (M)} \mathscr{F}_\psi \overset{\mathrm{Rot}(\boldsymbol{y}_\psi,\sigma)}{\rightarrow} \mathscr{F}_f, \quad (1)$$

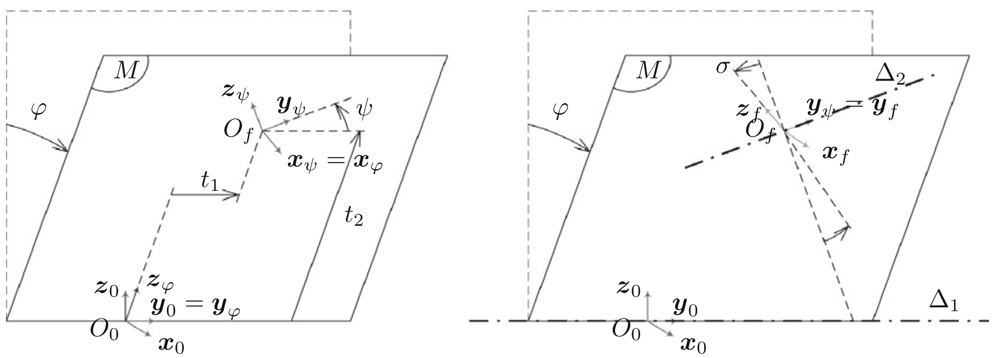

Fig. 1. Task decomposition.

where $\mathrm{Rot}(\boldsymbol{x},\theta)$ and $\mathrm{Tr}(\boldsymbol{x},t)$ respectively represent an $\boldsymbol{x}$-axis rotation of angle θ and an $\boldsymbol{x}$-axis translation of magnitude t. The reference frames $\mathscr{F}_\varphi$ and $\mathscr{F}_\psi$ are such that $\mathscr{F}_\varphi = (O_\varphi, \boldsymbol{x}_\varphi, \boldsymbol{y}_\varphi, \boldsymbol{z}_\varphi)$ and $\mathscr{F}_\psi = (O_\psi, \boldsymbol{x}_\psi, \boldsymbol{y}_\psi, \boldsymbol{z}_\psi)$ with $O_\varphi = O_0$, $O_\psi = O_f$, $\boldsymbol{y}_0 = \boldsymbol{y}_\varphi$, $\mathbf{x}_\varphi = \boldsymbol{x}_\psi$ and $\boldsymbol{y}_\psi = \boldsymbol{y}_f$.

2.2. Ideal form of solutions

From the presented decomposition scheme the desired mechanism can be obtained with a planar mechanism to orient and position a line (coordinates t_1, t_2 and ψ) in conjunction with a spatial mechanism to swivel the planar linkage (angle φ) and orient the line (angle σ). The function of the planar mechanism is to set the coordinates t_1, t_2 and ψ. The only planar 3-DOF mechanism with one independent loop is the 6-bar linkage [18]. The resulting kinematic chain is composed of six joints including possibly revolute or prismatic pairs. The moving platform can then be connected to the base with two RRR or RPR legs. The function of the spatial mechanism is then to set the remaining mobilities φ and σ that are obtained by adding the rotation axis Δ_1 and Δ_2 about $\boldsymbol{y}_0$ and $\boldsymbol{y}_f$, as described in Fig. 1. In theory, a rotative actuation about these two axes would suffice, but in practice this solution is not satisfactory as it generates important loads on the actuators. It is particularly noticeable for the motor attached to Δ_1, when an effort applied along the line is out of the plane (M). Instead, it is proposed to set the remaining mobilities φ and ψ with a third kinematic chain. The ideal architecture is presented in Fig. 2 using revolute and prismatic pairs. Notice that for modeling simplicity the joints connecting the two legs of the planar mechanism should intersect as well as the joints connecting the three legs to the platform. The architecture solution is shown with two UPU legs constituting the moving planar mechanism and a third SPU leg. This form of solution can be seen as ideal since there exists particular geometric conditions such as intersecting axes which lead to some simplifications in the kinematic models.

The mobility analysis of the third leg is presented hereafter. When the three parameters t_1, t_2 and ψ are set by the planar mechanism, the platform is connected to the ground by a first kinematic bond of mobility $m_1 = 2$ corresponding to the rotations about Δ_1 and Δ_2 and by a second kinematic bond relative to the third leg with a mobility $m_2 = 6$ that can be calculated with the Grübler's formula: $m = 6(n-j) + m_1 + m_2$ where $m = 2, n = 1$ and $j = 2$ represent the platform mobility, the number of moving links and kinematic bonds. It should be noted that the third leg is positioned some distance away from the plane $(O_0, \boldsymbol{x}_0, \boldsymbol{z}_0)$ which corresponds approximately to the CT image plane. Would the third leg be symmetrically attached to the base and the platform, the ideal form of architecture solution would be a 3-UPU mechanism with a U joint replacing the spherical joint of the third leg. The reason for this asymmetric arrangement of the third leg is mainly to avoid the presence of metal parts or electric devices in the CT plane and thus limit image artefacts.

According to the previous synthesis, we consider a 3T2R 5-DOF mechanism that allows: (1) to position a point O_f of a line whose axis is along vector $\boldsymbol{z}_f$; (2) to orient this line by two successive rotations parameterized by two angles α and β such that

$$\mathscr{F}_0 \xrightarrow{\mathrm{Rot}(\boldsymbol{x}_0,\alpha)} \mathscr{F}_\alpha \xrightarrow{\mathrm{Rot}(\boldsymbol{y}_0,\beta)} \mathscr{F}_f. \tag{2}$$

However, as explained in the next paragraph, practical conditions for intersecting axis and the use of prismatic joints were not met on the fabricated prototype leading to an alternative architecture.

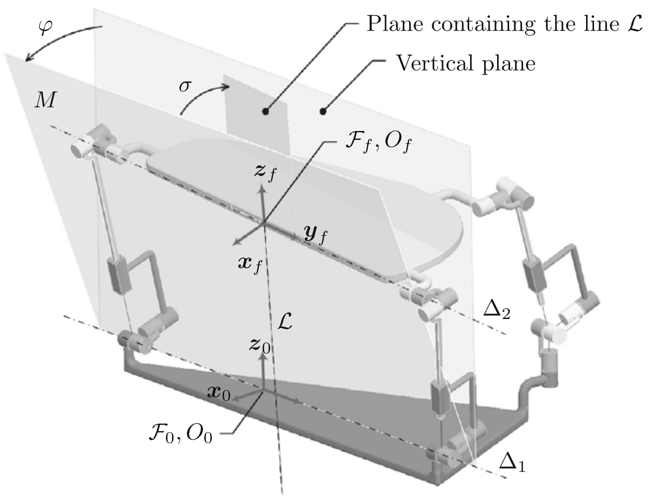

Fig. 2. Ideal form of architecture solution presented with 2-UPU and 1-SPU legs.

2.3. Proposed solution and fabricated prototype

From a kinematic viewpoint the most demanding specification for the mechanism is the needle angulation of 0–65° in the CT-scanner plane and ±25° in the perpendicular plane. The choice of actuators is central on the final architecture selection to provide a mechanism with reduced self-collisions and the required motion ranges. As linear actuators could not be integrated into the fabricated prototype due to their too large length in retracted position, specific actuation units were developed using rotary piezoelectric motors and so the prismatic joints of the UPU and SPU legs were replaced by revolute joints. Another concern relates to the selection of the actuated joints on the mechanism. There are at most 20 possibilities to locate the three actuators for the planar 6-bar linkage. However, placing motors on the two joints connected to the base link is impractical because the base link is attached to the patient and the motors would collide when the plane defined by the linkage swivel about a base line. Consequently, the remaining interesting possibilities for actuation are: S_1: $\mathrm{R\underline{RRR}RR}$, S_2: $\mathrm{R\underline{RR}R\underline{R}R}$, S_3: $\mathrm{R\underline{R}R\underline{RR}R}$ and S_4: $\mathrm{RR\underline{RRR}R}$. Among these closely resembling arrangements, the solution S_2 with two actuators on the first RRR chain and the last motor on the second chain has been selected. Concerning the third chain with a SRRR architecture, the actuated joints have been set to $\mathrm{S\underline{RR}R}$ to locate the motors after the spherical joint. It should be noted that the proposed mechanism is overconstrained since it features a full cycle mobility $m = 5$ while not satisfying the Grübler's general mobility criterion. The number h of overconstraints of a mechanism with n links and j kinematic parameters is $h = m + 6q - j$ where q denotes the number of independent kinematic loops that can be calculated as $q = j - n + 1$ [18].With the proposed mechanism we have $h = 1$ overconstraint coming from the first two 5R legs. For the prototype construction, this overconstraint has not been eliminated since it improves the global rigidity of the planar mechanism.

To limit self-collisions and allow actuators integration the axes of the revolute joints of the U pairs were offset as shown in Fig. 3a. Notice that having floating motors on the mechanism is not really a problem since the application only requires slow motions. The proposed parallel mechanism is finally composed of 16 revolute joints, five of which are actuated as indicated in Fig. 3a. With the proposed structure, the angles α and β respectively vary in the ranges 0–65° and ±25°, which is quite remarkable for a parallel robot. Fig. 3b shows the fabricated prototype of the mechanism in the CT-scanner ring with a needle guide mounted on the platform during an experimental evaluation of the system [2]. The geometric parameters of the constructed system are presented in the next section and the corresponding dimensions are provided in Table A.2.

3. System description

The following notational conventions will be used:

- the coordinates of a vector $\boldsymbol{AB}$, expressed in $\mathscr{F}_i$ are denoted as ${}^iAB$. Its components are ${}^iAB_{[x]}$, ${}^iAB_{[y]}$, ${}^iAB_{[z]}$ and its Euclidean norm is $\|\boldsymbol{AB}\|$.
- $c_i, s_i, t_i, c_{i,j}$ and $s_{i,j}$ are abbreviations for $\cos\theta_i, \sin\theta_i, \tan\frac{\theta_i}{2}, \cos(\theta_i+\theta_j)$ and $\sin(\theta_i+\theta_j)$ for any $i,j \in \mathbb{N}$.
- $\mathscr{J}_i$ refers to the joint coupling the $(i-1)$th link to the ith link. There are only revolute joints in the proposed mechanism. Their rotation axis are oriented as indicated by the arrows in Fig. 4.
- θ_i denotes the angular parameter of the joint $\mathscr{J}_i$. Depending on whether the joint is passive or actuated, parameter θ_i is respectively denoted by p_i or q_i.

A frame $\mathscr{F}_i$ is attached to each link and the homogeneous transformation between frames $\mathscr{F}_{i-1}$ and $\mathscr{F}_i$ is denoted by ${}^{i-1}T_i$. The corresponding rotation matrix is denoted as ${}^{i-1}R_i$. The reference position is denoted by ${}^{i-1}T_i(0)$ which corresponds to a simple configuration chosen for the successive links $i-1$ and i. In the following, it will be the initial fully extended configuration (see Fig. A.1) and every angular parameter θ_i will be measured with respect to its corresponding reference position

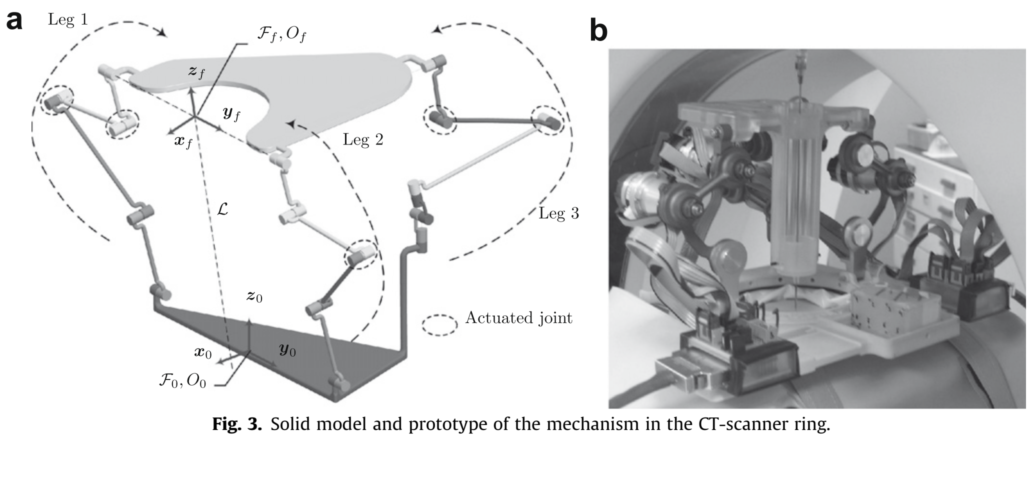

Fig. 3. Solid model and prototype of the mechanism in the CT-scanner ring.

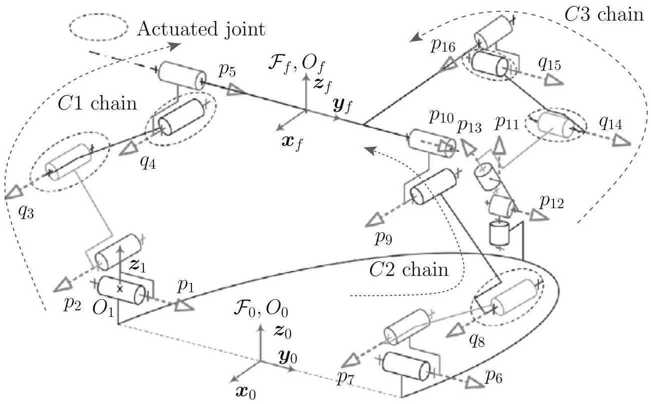

Fig. 4. Kinematic structure of the assembled mechanism.

${}^{i-1}T_i(0)$. The construction of homogeneous matrices is performed using the product of exponentials: the rigid transformation describing the pose of a frame $\mathscr{F}_i$ relative to $\mathscr{F}_{i-1}$ is

$$ {}^{i-1}T_i(\theta_i) = e^{\theta_i \widehat{\$}_{i/i-1}}\, {}^{i-1}T_i(0), \tag{3} $$

where $\widehat{\$}_{i/i-1}$ is the homogeneous matrix of the unit twist representing $\mathscr{J}_i$ [19]. To simplify both the reference position definition and calculations, rotation matrices at initial configuration are set to identities in ${}^{i-1}T_i(0)$.

The geometry of each leg, referred to as $C1, C2$ and $C3$, is precised in Table A.1. It should be noted that in the reference open-loop configuration of Fig. A.1, all the local frames are parallel to the base frame. Using relation (3) and the proposed parameterization, the homogeneous transformations of the serial kinematic chains $C1, C2$ and $C3$ can be evaluated. Upon loops closure (see Fig. 4), the chains $C1$ and $C2$ always stay in the (M)-plane defined by $(O_1, \boldsymbol{z}_1, \boldsymbol{y}_f)$. The base frame $\mathscr{F}_0$ and the platform frame $\mathscr{F}_f$ represented in this figure will be used in the next section for the position analysis of the chains $C1$ through $C3$.

4. Kinematic modeling

The position and the orientation of the platform with respect to the base could be represented with the homogeneous matrix ${}^0T_f$ or, with a minimal set of five parameters, using the position of O_f and the angles α and β defined by Eq. (2). For the following calculations, we introduce an alternative parameterization defined by the position of O_f and the vector $\boldsymbol{z}_f$ normal to the platform. The components of $\boldsymbol{z}_f$ in $\mathscr{F}_0$ can be obtained from the last column of the rotation matrix, i.e. ${}^0\boldsymbol{z}_f = [c\alpha s\beta \quad -s\alpha \quad c\alpha c\beta]^T$.

4.1. Inverse kinematics

The inverse kinematics problem can be stated as finding $[q_3 \quad q_4 \quad q_8 \quad q_{14} \quad q_{15}]^T$ such that, given the pose parameters ${}^0\boldsymbol{O}_0\boldsymbol{O}_f$ and ${}^0\boldsymbol{z}_f$

$$ {}^0T_f \begin{bmatrix} {}^f z_f \\ 0 \end{bmatrix} = \begin{bmatrix} {}^0\boldsymbol{z}_f \\ 0 \end{bmatrix}, \quad {}^0T_f \begin{bmatrix} {}^f\boldsymbol{O}_0\boldsymbol{O}_f \\ 0 \end{bmatrix} = \begin{bmatrix} {}^0\boldsymbol{O}_0\boldsymbol{O}_f \\ 0 \end{bmatrix}. \tag{4} $$

This problem is solved in three steps: calculation of (i) the parameters of $C1$ and $C2$ in the (M)-plane; (ii) the angle p_1 (or p_6) corresponding to the rotation about Δ_1; (iii) the parameters of $C3$.

4.1.1. Calculation of the sum $\Sigma_{2,3,4} = p_2 + q_3 + q_4$

The chains $C1$ and $C2$ are connected to the base via two revolute joints whose axes are coincident with Δ_1. Similarly, $C1$ and $C2$ are connected to the platform via two revolute joints whose axes are coincident with Δ_2 and orthogonal to $\boldsymbol{z}_f$. From this special arrangement of $C1$ and $C2$, it follows that $p_1 = p_6$ and $p_5 = p_{10}$, and that

$$ \boldsymbol{y}_5 \cdot \boldsymbol{z}_f = 0. \tag{5} $$

Upon calculation of the projection of $\boldsymbol{y}_5$ and $\boldsymbol{z}_f$ in $\mathscr{F}_1$, we obtain the following equations[1]

[1] The homogeneous matrix ${}^0T_f$ between the base and the platform, computed from the chain Ck, is written ${}^0T_{f|Ck}$.

$$ {}^{1}T_{2|C1}{}^{2}T_{3|C1}{}^{3}T_{4|C1}{}^{4}T_{5|C1}\begin{bmatrix} {}^{5}\boldsymbol{y}_5 \\ 0 \end{bmatrix} = \begin{bmatrix} 0 \\ c_{2,3,4} \\ s_{2,3,4} \\ 0 \end{bmatrix}, \quad {}^{1}T_{0|C1}\begin{bmatrix} {}^{0}\boldsymbol{z}_f \\ 0 \end{bmatrix} = \begin{bmatrix} {}^{0}\boldsymbol{z}_{f_{[x]}}c_1 - {}^{0}\boldsymbol{z}_{f_{[z]}}s_1 \\ {}^{0}\boldsymbol{z}_{f_{[y]}} \\ {}^{0}\boldsymbol{z}_{f_{[x]}}s_1 + {}^{0}\boldsymbol{z}_{f_{[z]}}c_1 \\ 0 \end{bmatrix}. \tag{6} $$

Eq. (5) can then be written ${}^{0}\boldsymbol{z}_{f\,[y]}c_{2,3,4} + ({}^{0}\boldsymbol{z}_{f_{[x]}}s_1 + {}^{0}\boldsymbol{z}_{f_{[z]}}c_1)s_{2,3,4} = 0$, from which one can obtain

$$ \Sigma_{2,3,4} = p_2 + q_3 + q_4 = \arctan 2\left(-{}^{0}\boldsymbol{z}_{f\,[y]}, {}^{0}\boldsymbol{z}_{f\,[x]}s_1 + {}^{0}\boldsymbol{z}_{f\,[z]}c_1\right), \tag{7} $$

where $\arctan 2$ is the two-argument arc tangent function defined in $[-\pi, \pi]$.

4.1.2. Calculation of the angles p_1, p_2, q_3 and q_4

Writing $\boldsymbol{O}_1\boldsymbol{O}_f$ via the two different paths $\mathscr{P}_1 = O_1 \to O_2 \to O_3 \to O_4 \to O_5 \to O_f$ and $\mathscr{P}_2 = O_1 \to O_0 \to O_f$ (see Fig. A.1) leads to

$$ \begin{aligned} &\boldsymbol{O}_1\boldsymbol{O}_f = \boldsymbol{O}_0\boldsymbol{O}_f - \boldsymbol{O}_0\boldsymbol{O}_1, \\ &a_2\boldsymbol{z}_1 + a_3\boldsymbol{z}_2 + a_4\boldsymbol{z}_3 + a_5\boldsymbol{z}_4 + a_6\boldsymbol{y}_5 = \boldsymbol{O}_0\boldsymbol{O}_f + a_0\boldsymbol{y}_0 - a_1\boldsymbol{z}_0, \end{aligned} \tag{8} $$

which can be projected in $\mathscr{F}_1$

$$ \begin{bmatrix} {}^{1}\boldsymbol{O}_1\boldsymbol{O}_f \\ 0 \end{bmatrix} = {}^{1}T_{2|C1}{}^{2}T_{3|C1}{}^{3}T_{4|C1}{}^{4}T_{5|C1}{}^{5}T_{f|C1}\begin{bmatrix} 0 \\ 1 \end{bmatrix} - \begin{bmatrix} 0 \\ 1 \end{bmatrix}, \tag{9} $$

$$ \begin{bmatrix} {}^{1}\boldsymbol{O}_0\boldsymbol{O}_f \\ 0 \end{bmatrix} - \begin{bmatrix} {}^{1}\boldsymbol{O}_0\boldsymbol{O}_1 \\ 0 \end{bmatrix} = {}^{1}T_{0|C1}\begin{bmatrix} {}^{0}\boldsymbol{O}_0\boldsymbol{O}_f - {}^{0}\boldsymbol{O}_0\boldsymbol{O}_1 \\ 0 \end{bmatrix}. \tag{10} $$

The resulting system of equations is then written as

$$ 0 = {}^{0}\boldsymbol{O}_0\boldsymbol{O}_{f\,[x]}c_1 - \left({}^{0}\boldsymbol{O}_0\boldsymbol{O}_{f\,[z]} - a_1\right)s_1, \tag{11} $$

$$ -a_3s_2 - a_4s_{2,3} - a_5s_{2,3,4} + a_6c_{2,3,4} = {}^{0}\boldsymbol{O}_0\boldsymbol{O}_{f\,[y]} + a_0, \tag{12} $$

$$ a_2 + a_3c_2 + a_4c_{2,3} + a_5c_{2,3,4} + a_6s_{2,3,4} = {}^{0}\boldsymbol{O}_0\boldsymbol{O}_{f\,[x]}s_1 + \left({}^{0}\boldsymbol{O}_0\boldsymbol{O}_{f\,[z]} - a_1\right)c_1. \tag{13} $$

The angle p_1 that fully describes the rotation of the (M)-plane about Δ_1 can be computed from Eq. (11). From the position of O_f in $\mathscr{F}_0$, we obtain

$$ p_1 = \arctan 2\left({}^{0}\boldsymbol{O}_0\boldsymbol{O}_{f\,[x]}, {}^{0}\boldsymbol{O}_0\boldsymbol{O}_{f\,[z]} - a_1\right). \tag{14} $$

To simplify further calculations, Eqs. (12) and (13) can be written as

$$ -a_3s_2 - a_4s_{2,3} = \mu_1, \tag{15} $$

$$ a_3c_2 + a_4c_{2,3} = \nu_1, \tag{16} $$

where μ_1 and ν_1 can be easily obtained from the previously computed terms. Then $a_3^2 + a_4^2 + 2a_3a_4c_3 = \mu_1^2 + \nu_1^2$ from which the solution for q_3 is

$$ q_3 = \pm\arccos\left(\frac{\mu_1^2 + \nu_1^2 - a_3^2 - a_4^2}{2a_3a_4}\right). \tag{17} $$

The preferred solution is chosen in order to have a larger available free space under the platform. In this case, we have $q_3 > 0$.

To calculate p_2 when q_3 is known, Eqs. (15) and (16) can be converted into a linear system with respect to s_2 and c_2 which results in

$$ s_2 = -\frac{(a_3 + a_4c_3)\mu_1 + a_4s_3\nu_1}{a_3^2 + a_4^2 + 2a_3a_4c_3}, \quad c_2 = -\frac{a_4s_3\mu_1 - (a_3 + a_4c_3)\nu_1}{a_3^2 + a_4^2 + 2a_3a_4c_3}. \tag{18} $$

The denominators are equal and positive and so p_2 can be determined as

$$ p_2 = \arctan 2\left(-(a_3 + a_4c_3)\mu_1 - a_4s_3\nu_1, -a_4s_3\mu_1 + (a_3 + a_4c_3)\nu_1\right). \tag{19} $$

Finally, the solution for q_4 can be computed as

$$ q_4 = \Sigma_{2,3,4} - p_2 - q_3. \tag{20} $$

4.1.3. Calculation of the angles p_7, q_8 and p_9

Due to the symmetric architecture of the 6-bar mechanism, the angles p_7, q_8 and p_9 of the chain $C2$ can be obtained analogously

$$p_7 = \arctan 2\big(-(a_3 + a_4c_8)\mu_2 - a_4s_8\nu_2, -a_4s_8\mu_2 + (a_3 + a_4c_8)\nu_2\big),$$
$$q_8 = \pm \arccos\left(\frac{\mu_2^2 + \nu_2^2 - a_3^2 - a_4^2}{2a_3a_4}\right),$$
$$p_9 = \arctan 2\left(-{}^0\boldsymbol{z}_{f\,[y]}, {}^0\boldsymbol{z}_{f\,[x]}s_1 + {}^0\boldsymbol{z}_{f\,[z]}c_1\right) - p_7 - q_8.$$

4.1.4. Angle between the platform and the (M)-plane

The last unknown for $C1$ and $C2$ is $p_5 = p_{10}$. Using the projection of $\boldsymbol{z}_f$ in $\mathscr{F}_1$ and the forward kinematics of the chain $C1$ or $C2$, it comes that

$${}^0\boldsymbol{z}_{f\,[x]}c_1 - {}^0\boldsymbol{z}_{f\,[z]}s_1 = s_5, \tag{21}$$
$${}^0\boldsymbol{z}_{f\,[y]} = -s_{2,3,4}c_5, \tag{22}$$
$${}^0\boldsymbol{z}_{f\,[x]}s_1 + {}^0\boldsymbol{z}_{f\,[z]}c_1 = c_{2,3,4}c_5. \tag{23}$$

Upon combining Eqs. (21)–(23), the expression of p_5 is written as

$$p_5 = \arctan 2\left({}^0\boldsymbol{z}_{f\,[x]}c_1 - {}^0\boldsymbol{z}_{f\,[z]}s_1, {}^0\boldsymbol{z}_{f\,[x]}s_1c_{2,3,4} - {}^0\boldsymbol{z}_{f\,[y]}s_{2,3,4} + {}^0\boldsymbol{z}_{f\,[z]}c_1c_{2,3,4}\right). \tag{24}$$

4.1.5. Study of C3

The last parameters to be calculated are those of the chain $C3$, namely $p_{11}, p_{12}, p_{13}, q_{14}, q_{15}$ and p_{16}. Starting from the platform, the arrangement of the first four links of the chain $C3$ is similar to those of the chains $C1$ or $C2$. The resolution for q_{14}, q_{15} and p_{16} can be performed analogously using a loop closure equation written from O_{16} to O_{11} via the chain $C3$ and the platform origin O_f. This equation is written $\boldsymbol{O}_{16}\boldsymbol{O}_{11} = \boldsymbol{O}_{16}\boldsymbol{O}_f + \boldsymbol{O}_0\boldsymbol{O}_{11} - \boldsymbol{O}_0\boldsymbol{O}_f$. The left-hand side of the previous equation can be calculated using $C3$ via the path $\mathscr{P}_3 = O_{16} \to O_{15} \to O_{14} \to O_{11}$ whereas its right-hand side corresponds to the path $\mathscr{P}_4 = O_{16} \to O_f \to O_0 \to O_{11}$, calculated using the known pose parameters. Upon performing the calculation of $\boldsymbol{O}_{16}\boldsymbol{O}_{11}$ in $\mathscr{F}_{16}$ via $\mathscr{P}_3$ and $\mathscr{P}_4$ it comes that

$${}^{16}\boldsymbol{O}_{16}\boldsymbol{O}_{11|\mathscr{P}_3} = \begin{bmatrix} b_3s_{14,15} + b_4s_{15} \\ -s_{16}(b_3c_{14,15} + b_4c_{15} + b_5) \\ -c_{16}(b_3c_{14,15} + b_4c_{15} + b_5) \end{bmatrix}, \tag{25}$$
$${}^{16}\boldsymbol{O}_{16}\boldsymbol{O}_{11|\mathscr{P}_4} = \begin{bmatrix} {}^{16}\boldsymbol{O}_{16}\boldsymbol{O}_{11\,[x]} \\ {}^{16}\boldsymbol{O}_{16}\boldsymbol{O}_{11\,[y]} \\ {}^{16}\boldsymbol{O}_{16}\boldsymbol{O}_{11\,[z]} \end{bmatrix} = \begin{bmatrix} -b_0c_\beta - b_2s_\beta + b_6 \\ -b_0s_\alpha s_\beta + b_1c_\alpha + b_2s_\alpha c_\beta - b_7 \\ -b_0c_\alpha s_\beta - b_1s_\alpha + b_2c_\alpha c_\beta - b_7 \end{bmatrix}. \tag{26}$$

A singularity appears when the term $b_3c_{14,15} + b_4c_{15} + b_5$ vanishes. This situation occurs when the line passing through O_{11} and O_{16} becomes orthogonal to the line passing through O_{15} and O_{16}, i.e. when $\boldsymbol{O}_{16}\boldsymbol{O}_{11} \cdot \boldsymbol{z}_{15} = 0$. In this particular configuration, the robot gains an idle DOF corresponding to a free rotation of the chain $C3$ about the line passing through O_{11} and O_{16}. When $b_3c_{14,15} + b_4c_{15} + b_5 \neq 0$, p_{16} can be calculated as

$$p_{16} = \arctan 2\big(-{}^{16}\boldsymbol{O}_{16}\boldsymbol{O}_{11\,[y]}, -{}^{16}\boldsymbol{O}_{16}\boldsymbol{O}_{11\,[z]}\big). \tag{27}$$

Next, one can observe that vector $\boldsymbol{O}_{16}\boldsymbol{O}_{11}$ is only parameterized by q_{14} and q_{15} and can be computed in $\mathscr{F}_{15}$ either using the known components of $\boldsymbol{O}_{16}\boldsymbol{O}_{11}$ in $\mathscr{F}_{16}$ or via $C3$. The resulting relations are written as

$$b_3s_{14,15} + b_4s_{15} = {}^{16}\boldsymbol{O}_{16}\boldsymbol{O}_{11\,[x]}, \tag{28}$$
$$0 = {}^{16}\boldsymbol{O}_{16}\boldsymbol{O}_{11\,[y]}c_{16} - {}^{16}\boldsymbol{O}_{16}\boldsymbol{O}_{11\,[z]}s_{16}, \tag{29}$$
$$-b_3c_{14,15} - b_4c_{15} = {}^{16}\boldsymbol{O}_{16}\boldsymbol{O}_{11\,[y]}s_{16} + {}^{16}\boldsymbol{O}_{16}\boldsymbol{O}_{11\,[z]}c_{16} + b_5. \tag{30}$$

These relations are analogous to Eqs. (11)–(13) and can be solved similarly. The angles q_{14} and q_{15} are computed as

$$q_{14} = \pm \arccos\left(\frac{\mu_3^2 + \nu_3^2 - b_3^2 - b_4^2}{2b_3b_4}\right), \tag{31}$$
$$q_{15} = \arctan 2\big((b_3c_{14} + b_4)\mu_3 + b_3\nu_3s_{14}, b_3\mu_3s_{14} - (b_3c_{14} + b_4)\nu_3\big). \tag{32}$$

where μ_3 and ν_3 are respectively the right-hand side terms of Eqs. (28) and (30). The preferred solution for q_{14} is chosen positive so as to obtain a configuration leaving O_{14} on the right of the line passing through O_{11} and O_{15}. Finally, the spherical joint parameters identification is completed by the inspection of the terms of the matrix ${}^0T_{13}$ evaluated via the paths $\mathscr{P}_5 = O_0 \to O_f \to O_{16} \to O_{15} \to O_{14} \to O_{13}$ and $\mathscr{P}_6 = O_0 \to O_{11} \to O_{12} \to O_{13}$. The homogeneous matrix ${}^0T_{13}$ calculated via $\mathscr{P}_5$ is a function of already known parameters from $C1$ and $C3$. When calculated via $\mathscr{P}_6$, ${}^0T_{13}$ is a function of the unknown parameters p_{11}, p_{12} and p_{13}

$$
{}^{0}T_{13|\mathscr{P}_6} = \begin{bmatrix} c_{11}c_{12} & -s_{11}c_{13}+c_{11}s_{12}s_{13} & s_{11}s_{13}+c_{11}s_{12}c_{13} & -b_0 \\ s_{11}c_{12} & c_{11}c_{13}+s_{11}s_{12}s_{13} & -c_{11}s_{13}+s_{11}s_{12}c_{13} & b_1 \\ -s_{12} & c_{12}s_{13} & c_{12}c_{13} & b_2 \\ 0 & 0 & 0 & 1 \end{bmatrix}. \tag{33}
$$

This homogeneous matrix corresponds to a ZYX-Euler angles convention whose parameters are

$$
\begin{aligned}
p_{12} &= \arctan 2\left(-{}^{0}T_{13[3,1]}, \sqrt{{}^{0}T^2_{13[3,2]} + {}^{0}T^2_{13[3,3]}}\right),\\
p_{11} &= \arctan 2\left({}^{0}T_{13[2,1]}, {}^{0}T_{13[1,1]}\right),\\
p_{13} &= \arctan 2\left({}^{0}T_{13[3,2]}, {}^{0}T_{13[3,3]}\right)
\end{aligned} \tag{34}
$$

provided that $p_{12} \neq \pm\frac{\pi}{2}$. If $p_{12} = \pm\frac{\pi}{2}$ the solution of Eq. (34) degenerates and only the sum or the difference of p_{11} and p_{13} can be computed. One possible convention is then to choose $p_{11} = 0$, and a solution can be calculated $p_{13} = \arctan 2\left({}^{0}T_{13[1,2]}, {}^{0}T_{13[2,2]}\right)$.

4.2. System workspace analysis

First, the reachable workspace of a wire model of the robot has been built. It represents the set of locations of the reference point O_f that may be reached with at least one orientation of the platform [20]. The construction has been achieved with a discretization of the pose parameters using a regular grid with steps of 1 mm for the position and 10° for the orientation. As joints limits and interferences between links are not taken into account, it only illustrates the theoretical reachable workspace of the mechanism. Fig. 5 pictures the half reachable workspace. The whole workspace is approximately hemispherical as prescribed by the application. In the case of a needle insertion task, the points O_0 and O_f can be seen respectively as the entry point on the patient's body and a grasping point on the instrument. Since the needle insertion is performed by an additional device mounted on its platform the distance between O_0 and O_f remains constant and it is more important to determine the orientation workspace, defined as the set of the possible orientations of the robot about O_0. In Fig. 5 the orientation workspace of the robot is presented. It has been sampled over the ranges [0°, 65°] and ±25° for the orientation angles as defined in paragraph 2.3. A 130 mm radius sphere is superimposed to show the average working height of the robot platform.

Because of the robot compactness, self-collisions between different parts of the robot may happen and it is of key importance to prevent them. The CAD model of the prototype together with the OPCODE collision engine [21] have been used to generate the robot sampled configuration space and check that it is constituted by connected compact sets, though this is not formally proven by such a discrete construction. This result, which is dependent of the prototype building is presented in [2].

4.3. Forward kinematics

The forward kinematics problem may be stated as finding all the possible pose parameters ${}^{0}\boldsymbol{O}_0\boldsymbol{O}_f$ and ${}^{0}\boldsymbol{z}_f$ corresponding to the values of the actuated joints angles q_3, q_4, q_8, q_{14} and q_{15}. It is well established that the forward kinematics of a parallel manipulator is generally a difficult problem with multiple solutions.

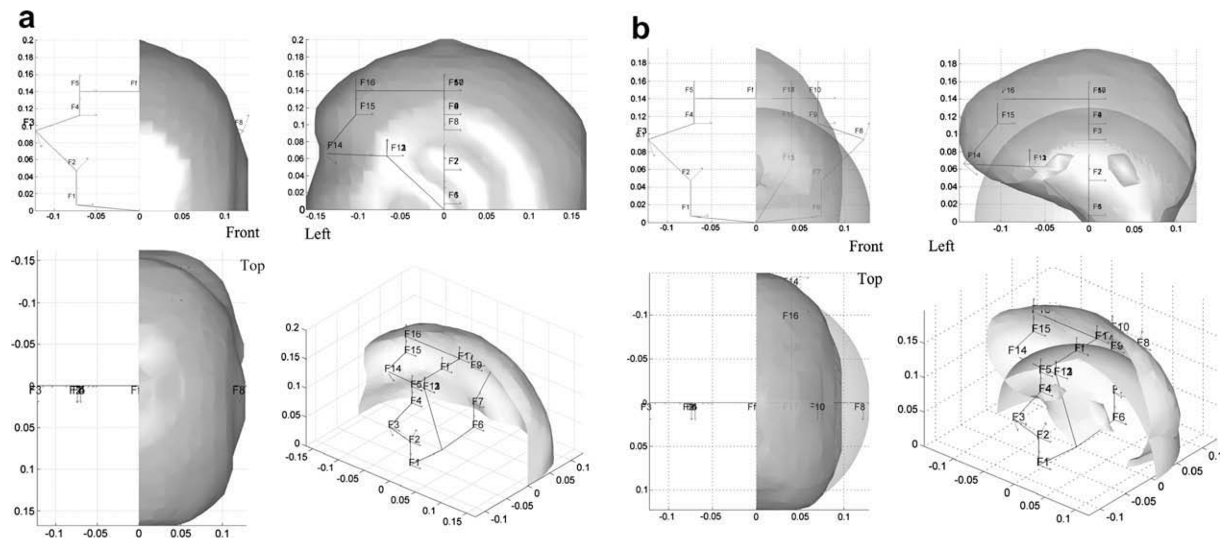

Fig. 5. (a) Reachable and (b) orientation workspace with the wire model.

4.3.1. Study of C1 and C2 in the (M)-plane

For the given values of the actuated joints angles q_3, q_4 and q_8, the objective is to compute the passive joint angles p_2, p_7 and p_9 of the planar mechanism constituted by $C1$ and $C2$. Suppose that the kinematic loop has virtually been opened at the joint $\mathscr{J}_9$. With the remaining passive joints, the curves generated by O_9 in the full range of motion of the two sub-assemblies are two circles centered about O_2 and O_7. The solution for the passive angles p_2, p_7 and p_9 can be obtained by determining the intersection of these two circles. With the geometry of the problem in mind, algebraic solution can be developed accordingly.

The projections of $\boldsymbol{O}_2\boldsymbol{O}_9$ in $\mathscr{F}_1$ computed via $C1$ and $C2$ are

$$ {}^1\boldsymbol{O}_2\boldsymbol{O}_{9|C1} = \begin{bmatrix} 0 \\ -a_3s_2 - a_4s_{2,3} + 2a_6c_{2,3,4} \\ a_3c_2 + a_4c_{2,3} + 2a_6s_{2,3,4} \end{bmatrix}, \quad {}^1\boldsymbol{O}_2\boldsymbol{O}_{9|C2} = \begin{bmatrix} 0 \\ 2a_0 - a_3s_7 - a_4s_{7,8} \\ a_3c_7 + a_4c_{7,8} \end{bmatrix}. \tag{35} $$

Equating the squared norm of both expressions (see (A.2)) leads to a transcendental equation of the form

$$ \mu_4c_7 + \nu_4s_7 + \gamma_4 = 0, \tag{36} $$

which can be solved classically using $t_7 = \tan\frac{p_7}{2}$

$$ t_7 = \frac{\nu_4 \pm \sqrt{\mu_4^2 + \nu_4^2 - \gamma_4^2}}{\mu_4 - \gamma_4}. \tag{37} $$

Depending on the sign of $\delta_4 = \mu_4^2 + \nu_4^2 - \gamma_4^2$, there are three possible cases:

(i) if $\delta_4 < 0$, there is no solution to the forward kinematics (the radius of both circles are too small and thus the mechanism cannot be assembled);
(ii) if $\delta_4 = 0$, there is a unique solution (the circles are tangent to each other) and O_9 is on the line passing through O_2 and O_7;
(iii) if $\delta_4 > 0$, which is generally the case, both solutions are valid with the platform either above or beneath the line passing through O_2 and O_7.

Hence, when $\delta_4 \geqslant 0$

$$ p_7 = 2\arctan\left(\frac{\nu_4 \pm \sqrt{\delta_4}}{\mu_4 - \gamma_4}\right). \tag{38} $$

In normal conditions, the platform should be above the line passing through O_2 and O_7, which can be restated as $\boldsymbol{O}_2\boldsymbol{O}_9 \cdot \boldsymbol{z}_1 > 0$. Then, from Eq. (35) right, p_7 should be chosen so that it verifies

$$ (a_3 + a_4c_8)c_7 - a_4s_8s_7 > 0. \tag{39} $$

As a consequence, the mechanism has only one assembly mode that verifies the aforementioned condition.

When p_7 is known Eq. (35) can be combined to form a system of linear equations in s_2 and c_2 that can be solved to determine

$$ p_2 = \arctan 2\big(-(a_3 + a_4c_3 + 2a_6s_{3,4})\mu_5 - (a_4s_3 - 2a_6c_{3,4})\nu_5, -(a_4s_3 - 2a_6c_{3,4})\mu_5 + (a_3 + a_4c_3 + 2a_6s_{3,4})\nu_5\big), \tag{40} $$

where $\mu_5 = 2a_0 - a_3s_7 - a_4s_{7,8}$ and $\nu_5 = a_3c_7 + a_4c_{7,8}$.

Finally, the solution for q_9 can be computed as

$$ p_9 = p_2 + q_3 + q_4 - p_7 - q_8. \tag{41} $$

As expected, controlling the parameters q_3, q_4 and q_8 constrains the first three DOF but p_1 (or p_6) and p_5 (or p_{10}) are still to be found.

4.3.2. Loop closure with C3

Suppose that the mechanism formed by $C1$, $C2$ and $C3$ is opened at point O_{17}. The locus of O_{17} is a circle $\mathscr{C}_1$ about $\mathscr{J}_1$ with a fixed radius when the planar mechanism composed of $C1$ and $C2$ rotates about the passive joint $\mathscr{J}_1$. Besides, when q_{14} and q_{15} are fixed, the locus of O_{17} is a sphere $\mathscr{S}_1$ centered on O_{11} with radius $\|\boldsymbol{O}_{11}\boldsymbol{O}_{17}\|$. The assembly modes correspond to the intersections between the sphere and the circle which are either two points or a single point (circle tangent to the sphere) or an empty set (radii too small). This geometric property of the mechanism can be formulated algebraically in writing that the squared norm of $\boldsymbol{O}_{11}\boldsymbol{O}_{17}$ can be calculated via the chains $C1$ and $C3$ with the paths $\mathscr{P}_7 = O_{11} \to O_0 \to O_1 \to O_2 \to O_3 \to O_4 \to O_5 \to O_{17}$ and $\mathscr{P}_8 = O_{11} \to O_{14} \to O_{15} \to O_{16} \to O_{17}$

$$ ||\boldsymbol{O}_{11}\boldsymbol{O}_{17|\mathscr{P}_7}||^2 - ||\boldsymbol{O}_{11}\boldsymbol{O}_{17|\mathscr{P}_8}||^2 = 0. \tag{42} $$

The simplest forms of the components of $\boldsymbol{O}_{11}\boldsymbol{O}_{17|\mathscr{P}_7}$ and $\boldsymbol{O}_{11}\boldsymbol{O}_{17|\mathscr{P}_8}$ are respectively obtained with a projection in $\mathscr{F}_0$ and $\mathscr{F}_{13}$. The development of Eq. (42) takes the form (see (A.2))

$$\mu_6 c_1 + \nu_6 s_1 + \gamma_6 = 0, \tag{43}$$

which is solved for p_1 in the same way as previously for p_7. When $\delta_6 = \mu_6^2 + \nu_6^2 - \gamma_6^2$ is positive, two real solutions for p_1 can be calculated

$$p_1 = 2\arctan\left(\frac{\nu_6 \pm \sqrt{\delta_6}}{\mu_6 - \gamma_6}\right). \tag{44}$$

They correspond to assembly modes which are symmetric with respect to the plane passing through O_{11} and the axis of $\mathscr{J}_1$. In normal conditions, the platform should be above the aforementioned plane which can be formulated as $(\boldsymbol{y}_1 \times \boldsymbol{O}_1\boldsymbol{O}_{11}) \cdot \boldsymbol{O}_{11}\boldsymbol{O}_{17} \geqslant 0$ or, equivalently $(\boldsymbol{y}_1 \times \boldsymbol{O}_1\boldsymbol{O}_{11}) \cdot \boldsymbol{z}_1 \geqslant 0$ or $-\boldsymbol{x}_1 \cdot \boldsymbol{O}_1\boldsymbol{O}_{11} \geqslant 0$ which yields

$$b_0 c_1 + (b_2 - a_1)s_1 \geqslant 0. \tag{45}$$

Thus, p_1 should be chosen so that it verifies relation (45), resulting in one single assembly mode.

Once p_1 is chosen, the platform orientation p_5 still has to be identified. Now suppose that the mechanism is opened at point O_{16}. The locus of O_{16} is a circle $\mathscr{C}_2$ about the axis of $\mathscr{J}_5$, with a fixed radius, when the platform rotates about the passive joint $\mathscr{J}_5$. Besides, when q_{14} and q_{15} are fixed, the locus of O_{16} is a sphere $\mathscr{S}_2$ centered on O_{11} with radius $\|\boldsymbol{O}_{11}\boldsymbol{O}_{16}\|$. As a valid assembly mode existed for the mechanism with the previously chosen value of p_1, the intersection between the sphere $\mathscr{S}_2$ and the circle $\mathscr{C}_2$ is either a single point (circle tangent to the sphere) or two points. These last two solutions correspond to assembly modes of the robot which are symmetric with respect to the plane passing through O_{11} and the axis of $\mathscr{J}_5$. In the same way as for p_1, the geometric property of the mechanism yields an equation analogous to (42) in which O_{17} is replaced by O_{16}. Its comes that

$$\mu_7 c_5 + \nu_7 s_5 + \gamma_7 = 0, \tag{46}$$

where μ_7, ν_7 and γ_7 can be calculated from the already known parameters (see (A.2)), which is then solved for p_5 to obtain

$$p_5 = 2\arctan\left(\frac{\nu_7 \pm \sqrt{\mu_7^2 + \nu_7^2 - \gamma_7^2}}{\mu_7 - \gamma_7}\right). \tag{47}$$

These two solutions correspond to assembly modes of the robot which are symmetric with respect to the plane passing through O_{11} and the axis of $\mathscr{J}_5$. In normal conditions, the platform should be above the aforementioned plane. This condition can be formulated as $(\boldsymbol{y}_5 \times \boldsymbol{O}_{11}\boldsymbol{O}_{17}) \cdot \boldsymbol{O}_{16}\boldsymbol{O}_{17} \geqslant 0$ or, equivalently $(\boldsymbol{y}_5 \times \boldsymbol{O}_{11}\boldsymbol{O}_{17}) \cdot \boldsymbol{x}_5 \geqslant 0$ or $\boldsymbol{z}_5 \cdot \boldsymbol{O}_{11}\boldsymbol{O}_{17} \geqslant 0$ which yields a relation of the form

$$\mu_8 c_5 + \nu_8 s_5 \geqslant 0, \tag{48}$$

where μ_8 and ν_8 can be calculated from the already known terms. Hence, p_5 should be chosen so that it verifies relation (48), resulting in one single assembly mode.

Finally, the total number of assembly modes is $2^3 = 8$ solutions. but limitations such as mechanical stops or self-collisions eliminate some of them. The constraints corresponding to Eqs. (39), (45) and (48) limit the choice to a unique assembly mode which complies with the practical limitations. At last, the pose parameters can be calculated as follows

$$^0\boldsymbol{z}_f = \begin{bmatrix} c_1 s_5 + s_1 c_{2,3,4} c_5 \\ -s_{2,3,4} c_5 \\ -s_1 s_5 + c_1 c_{2,3,4} c_5 \end{bmatrix}, \quad {}^0\boldsymbol{O}_0\boldsymbol{O}_f = \begin{bmatrix} (a_2 + a_3 c_2 + a_4 c_{2,3} + a_5 c_{2,3,4} + a_6 s_{2,3,4}) s_1 \\ -a_0 - a_3 s_2 - a_4 s_{2,3} - a_5 s_{2,3,4} + a_6 c_{2,3,4} \\ a_1 + (a_2 + a_3 c_2 + a_4 c_{2,3} + a_5 c_{2,3,4} + a_6 s_{2,3,4}) c_1 \end{bmatrix}. \tag{49}$$

5. Conclusion

In this paper, a novel 5-DOF parallel system has been presented. It has been originally designed to cope with the constraints of body mounted robots for CT-guided interventions More generally, the proposed mechanical structure is suitable to achieve tasks which do not require self-rotation of the robot platform. The special asymmetric arrangement of the legs enables a wide range of evolution for the needle angulation. The system mobility has been obtained using only revolute joints and rotary actuators which simplifies the robot building. The closed-form inverse and forward kinematic models have been derived using a geometrical approach. Explicit conditions for assembly modes selection have also been presented. Ongoing tasks on this structure include the calculation of the system Jacobian matrix which opens perspectives in terms of analysis and control. From the differential model, the study of the system singularities will possibly be coped, for instance by considering interval analysis methods [22], though at the moment it remains a largely open problem.

Acknowledgements

The authors wish to thank the Alsace Region and the CNRS-ROBEA program for the financial support of this research work, and Pr. Afshin Gangi for his medical expertise and for his constant enthusiasm.

Appendix A

A.1. Joints screw axis, reference frames and dimensional parameters

The last rows in Table A.1 indicate the location of the origin O_f of the platform frame $\mathscr{F}_f$ with respect to the base frame $\mathscr{F}_0$.

A.2. Intermediate calculation steps

To improve the text readability, some intermediate calculation steps are given hereafter.
In paragraph 4.3.1 the developed version of Eq. (36) gives μ_4, v_4 and γ_4

$$4a_0^2 + a_3^2 + a_4^2 - 4a_0a_3s_7 - 4a_0a_4s_{7,8} + 2a_3a_4c_8 = a_3^2 + a_4^2 + 4a_6^2 + 2a_3a_4c_3 + 4a_3a_6s_{3,4} + 4a_4a_6s_4. \tag{A.1}$$

Table A.1
Screw axis for the chains $C1/C2$ (up) and $C3$ (bottom) in the position of Fig. A.1.

Frame	Position ${}^0\boldsymbol{O}_0\boldsymbol{O}_i$	Axis	Ang. Par.	Frame	Position ${}^0\boldsymbol{O}_0\boldsymbol{O}_i$	Axis	Ang. Par.
$\mathscr{F}_1$	$[0\ -a_0\ a_1]^T$	$[0\ 1\ 0]^T$	p_1	$\mathscr{F}_6$	$[0\ a_0\ a_1]^T$	$[0\ 1\ 0]^T$	p_6
$\mathscr{F}_2$	$[0\ -a_0\ \sum_{j=1}^{2}a_j]^T$	$[1\ 0\ 0]^T$	p_2	$\mathscr{F}_7$	$[0\ a_0\ \sum_{j=1}^{2}a_j]^T$	$[1\ 0\ 0]^T$	p_7
$\mathscr{F}_3$	$[0\ -a_0\ \sum_{j=1}^{3}a_j]^T$	$[1\ 0\ 0]^T$	q_3	$\mathscr{F}_8$	$[0\ a_0\ \sum_{j=1}^{3}a_j]^T$	$[1\ 0\ 0]^T$	q_8
$\mathscr{F}_4$	$[0\ -a_0\ \sum_{j=1}^{4}a_j]^T$	$[1\ 0\ 0]^T$	q_4	$\mathscr{F}_9$	$[0\ a_0\ \sum_{j=1}^{4}a_j]^T$	$[1\ 0\ 0]^T$	p_9
$\mathscr{F}_5$	$[0\ -a_0\ \sum_{j=1}^{5}a_j]^T$	$[0\ 1\ 0]^T$	p_5	$\mathscr{F}_{10}$	$[0\ a_0\ \sum_{j=1}^{5}a_j]^T$	$[0\ 1\ 0]^T$	p_{10}
$\mathscr{F}_f$	$[0\ -a_0+a_6\ \sum_{j=1}^{5}a_j]^T$			$\mathscr{F}_f$	$[0\ a_0-a_6\ \sum_{j=1}^{5}a_j]^T$		

Frame	Position ${}^0\boldsymbol{O}_0\boldsymbol{O}_i$	Axis	Ang. Par.
$\mathscr{F}_{11}$	$[-b_0\ b_1\ b_2]^T$	$[0\ 0\ 1]^T$	p_{11}
$\mathscr{F}_{12}$	$[-b_0\ b_1\ b_2]^T$	$[0\ 1\ 0]^T$	p_{12}
$\mathscr{F}_{13}$	$[-b_0\ b_1\ b_2]^T$	$[1\ 0\ 0]^T$	p_{13}
$\mathscr{F}_{14}$	$[-b_0\ b_1\ \sum_{j=2}^{3}b_j]^T$	$[0\ 1\ 0]^T$	q_{14}
$\mathscr{F}_{15}$	$[-b_0\ b_1\ \sum_{j=2}^{4}b_j]^T$	$[0\ 1\ 0]^T$	q_{15}
$\mathscr{F}_{16}$	$[-b_0\ b_1\ \sum_{j=2}^{5}b_j]^T$	$[1\ 0\ 0]^T$	p_{16}
$\mathscr{F}_f$	$[-b_0+b_6\ b_1-b_7\ \sum_{j=2}^{5}b_j]^T$		

Table A.2
Dimensional parameters values used for the constructed prototype.

Parameter i	0	1	2	3	4	5	6	7
a_i (mm)	73.8	7.0	40.0	67.0	55.0	28.0	70.0	
b_i (mm)	67.6	40.0	63.0	75.0	60.0	28.0	104.0	40.0

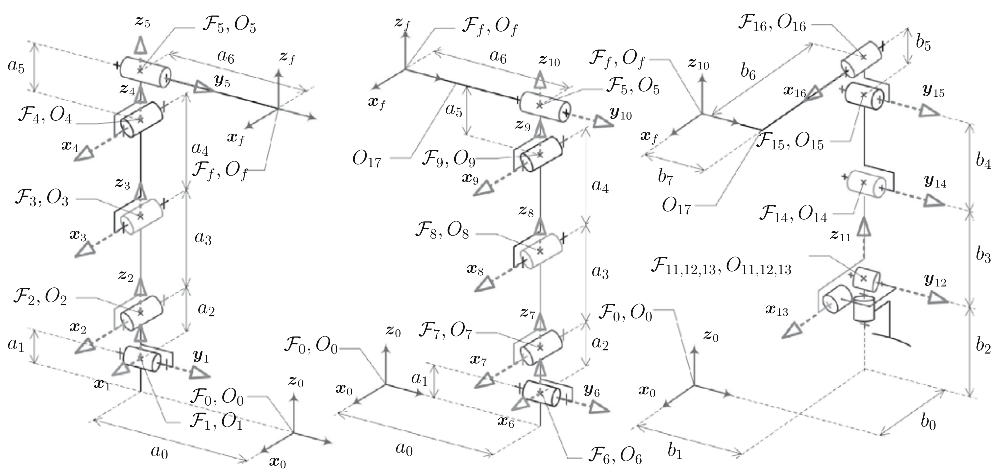

Fig. A.1. Screw axis definition for chains $C1$, $C2$ and $C3$ sketched in reference position.

In paragraph 4.3.2 the developed version of Eq. (43) gives μ_6, ν_6 and γ_6

$$\begin{aligned}
&2(a_1-b_2)(a_5c_{2,3,4}+a_6s_{2,3,4}+b_7s_{2,3,4}+a_4c_{2,3}+a_3c_2+a_2)c_1\\
&\quad+2b_0(a_2+a_3c_2+a_4c_{2,3}+a_5c_{2,3,4}+a_6s_{2,3,4}+b_7s_{2,3,4})s_1+(a_1-b_2)^2+b_0^2\\
&\quad+(-a_0-a_3s_2-a_4s_{2,3,4}-a_5s_{2,3,4}+a_6c_{2,3,4}-b_1+b_7c_{2,3,4})^2+(a_2+a_3c_2+a_4c_{2,3}+a_5c_{2,3,4}+a_6s_{2,3,4}+b_7s_{2,3,4})^2\\
&\quad-(b_4s_{14}+b_5s_{14,15}+b_6c_{14,15})^2-(b_3+b_4c_{14,15}+b_5c_{14,15}-b_6s_{14,15})^2=0.
\end{aligned}\tag{A.2}$$

In paragraph 4.3.2 the developed version of Eq. (46) gives μ_7, ν_7 and γ_7

$$\begin{aligned}
&(b_0c_1+(b_2-a_1)s_1-b_6c_5)^2+(-a_0-a_3s_2-a_4s_{2,3}-a_5s_{2,3,4}+a_6c_{2,3,4}-b_1-b_6s_{2,3,4}s_5+b_7c_{2,3,4})^2\\
&\quad+(a_2+a_3c_2+a_4c_{2,3}+a_5c_{2,3,4}+a_6s_{2,3,4}+b_0s_1+b_6c_{2,3,4}s_5+b_7s_{2,3,4}+(a_1-b_2)c_1)^2\\
&\quad-(b_4s_{14}+b_5s_{14,15})^2-(b_3+b_4c_{14}+b_5c_{14,15})^2=0.
\end{aligned}\tag{A.3}$$

References

[1] B. Maurin, O. Piccin, B. Bayle, J. Gangloff, M. de Mathelin, A parallel 5 DOF positioner for semi-spherical workspaces, in: Proceedings of the 2004 ASME Design Engineering Technical Conferences, Salt Lake City, USA, 2004.
[2] B. Maurin, B. Bayle, O. Piccin, J. Gangloff, M. de Mathelin, P. Zanne, C. Doignon, A. Gangi, A patient-mounted robotic platform for CT-scan guided procedures, IEEE Transactions on Biomedical Engineering 55 (10) (2008) 2417–2425.
[3] D. Stoianovici, J.A. Cadeddu, R.D. Demaree, H.A. Basile, R.H. Taylor, L.L. Whitcomb, L.R. Kavoussi, A novel mechanical transmission applied to percutaneous renal access, Proceedings of the ASME Dynamic Systems and Control Division DSC 61 (1997) 401–406.
[4] D. Stoianovici, K. Cleary, A. Patriciu, D. Mazilu, A. Stanimir, N. Craciunoiu, V. Watson, L. Kavoussi, AcuBot: a robot for radiological interventions, IEEE Transactions on Robotics and Automation 19 (5) (2003) 927–930.
[5] A. Melzer, B. Gutmann, A. Lukoschek, M. Mark, Experimental evaluation of an MRI compatible telerobotic system for CT MRI guided interventions, Supplement to Radiology (2003) 226–409.
[6] G. Kronreif, M. Fürst, J. Kettenbach, M. Figl, R. Hanel, Robotic guidance for percutaneous interventions, Journal of Advanced Robotics 17 (6) (2003) 541–560.
[7] A. Vilchis, J. Troccaz, P. Cinquin, K. Masuda, F. Pelissier, A new robot architecture for tele-echography, IEEE Transactions on Robotics and Automation 19 (5) (2003) 922–926.
[8] D. Stoianovici, D. Song, D. Petrisor, D. Ursu, D. Mazilu, M. Mutener, M. Schar, A. Patriciu, "MRI stealth" robot for prostate interventions, Minimally Invasive Therapy and Allied Technologies 16 (4) (2007) 241–248.
[9] B. Maurin, J. Gangloff, B. Bayle, M. de Mathelin, O. Piccin, P. Zanne, C. Doignon, L. Soler, A. Gangi, A parallel robotic system with force sensors for percutaneous procedures under CT-guidance, in: Medical Image Computing and Computer-Assisted Intervention Conference, St-Malo, France, 2004, pp. 176–183.
[10] F. Gao, W. Li, X. Zhao, Z. Jin, H. Zhao, New kinematic structures for 2-, 3-, 4-, and 5-DOF parallel manipulator designs, Mechanism and Machine Theory 37 (11) (2002) 1395–1411.
[11] Z. Huang, Q. Li, Type synthesis of symmetrical lower-mobility parallel mechanisms using the constraint-synthesis method, The International Journal of Robotics Research 22 (1) (2003) 59–79.
[12] M.J. Liu, G.Z. Li, A geometric theory for synthesis and analysis of sub-6 DOF parallel manipulators, IEEE International Conference on Robotics and Automation (2005) 2938–2943.
[13] Y. Fang, L.W. Tsai, Structure synthesis of a class of 4-DOF and 5-DOF parallel manipulators with identical limb structures, Journal of Robotics Research 21 (9) (2002) 799–810.
[14] Q. Li, Z. Huang, J. Hervé, Type synthesis of 3R2T 5-DOF parallel mechanisms using the Lie group of displacements, IEEE Transactions on Robotics and Automation 20 (2) (2004) 173–180.
[15] X. Kong, C. Gosselin, Type synthesis of 5-DOF parallel manipulators based on screw theory, Journal of Robotic Systems 22 (2005) 535–547.
[16] J. Hervé, The Lie group of rigid body displacements, a fundamental tool for mechanism design, Mechanism and Machine Theory 34 (1999) 719–730.
[17] J. Angeles, The qualitative synthesis of parallel manipulators, Journal of Mechanical Design 126 (4) (2004) 617–624.
[18] L.W. Tsai, Mechanism Design: Enumeration of Kinematic Structures According to Function, Mechanical Engineering Series, CRC Press, 2001.
[19] R.M. Murray, Z. Li, S.S. Sastry, A Mathematical Introduction to Robotic Manipulation, CRC Press, 1994.
[20] J.-P. Merlet, Parallel Robots, second ed., Springer, 2006.
[21] P. Terdiman, OPCODE 1.3 – optimized collision detection, 2003. <http://www.codercorner.com/Opcode.htm>.
[22] J.-P. Merlet, Optimal design of robots, in: Robotics: Science and systems, MIT, Boston, USA, 2005.